Structure of Bovine Pancreatic Cholesterol Esterase at 1.6 Å: Novel Structural Features Involved in Lipase Activation[†,‡]

Julian C.-H. Chen,[§] Larry J. W. Miercke,[||] Jolanta Krucinski,[||] Jacqueline R. Starr,[⊥,#] Gina Saenz,[⊥,@] Xingbo Wang,[⊥] Curtis A. Spilburg,[⊥,+] Louis G. Lange,[⊥] Jeff L. Ellsworth,[⊥,○] and Robert M. Stroud*[,||]

Graduate Group in Biophysics and Department of Biochemistry and Biophysics, University of California, San Francisco, California 94143, and CV Therapeutics, Inc., 3172 Porter Drive, Palo Alto, California 94306

Received December 4, 1997; Revised Manuscript Received February 4, 1998

ABSTRACT: The structure of pancreatic cholesterol esterase, an enzyme that hydrolyzes a wide variety of dietary lipids, mediates the absorption of cholesterol esters, and is dependent on bile salts for optimal activity, is determined to 1.6 Å resolution. A full-length construct, mutated to eliminate two N-linked glycosylation sites (N187Q/N361Q), was expressed in HEK 293 cells. Enzymatic activity assays show that the purified, recombinant, mutant enzyme has activity identical to that of the native, glycosylated enzyme purified from bovine pancreas. The mutant enzyme is monomeric and exhibits improved homogeneity which aided in the growth of well-diffracting crystals. Crystals of the mutant enzyme grew in space group *C*2, with the following cell dimensions: $a = 100.42$ Å, $b = 54.25$ Å, $c = 106.34$ Å, and $\beta = 104.12°$, with a monomer in the asymmetric unit. The high-resolution crystal structure of bovine pancreatic cholesterol esterase ($R_{cryst} = 21.1\%$; $R_{free} = 25.0\%$ to 1.6 Å resolution) shows an $\alpha-\beta$ hydrolase fold with an unusual active site environment around the catalytic triad. The hydrophobic C terminus of the protein is lodged in the active site, diverting the oxyanion hole away from the productive binding site and the catalytic Ser194. The amphipathic, helical lid found in other triglyceride lipases is truncated in the structure of cholesterol esterase and therefore is not a salient feature of activation of this lipase. These two structural features, along with the bile salt-dependent activity of the enzyme, implicate a new mode of lipase activation.

Pancreatic cholesterol esterase (CEase[1]), also known as bile salt-activated lipase, is responsible for the hydrolysis of dietary cholesterol esters, fat soluble vitamin esters, phospholipids, and triglycerides (*1*, *2*). As such, it is one of the central enzymes that mediates absorption of dietary lipids through the intestinal wall into the bloodstream. A number of studies have suggested a possible role for CEase in the absorption of free cholesterol at the brush border membrane of the small intestine (*3*−*6*), though a CEase gene knockout showed little change in the absorption of cholesterol (*7*). CEase is present in high concentrations in breast milk and plays a crucial role in development by supplying the enzyme to infants whose pancreases are not yet fully developed (*1*, *2*). A role has also been demonstrated for CEase in the hepatic uptake of HDL-associated cholesterol esters (*8*). The bile salt dependence of enzymatic activity identifies CEase as a distinct lipase with necessarily different structural changes upon activation.

Bovine pancreatic CEase is a glycoprotein of 579 amino acids, with a notable proline-rich region between amino acids 540 and 573, and a highly conserved six-amino acid hydrophobic sequence forming the extreme C terminus of the protein (*9*). The proline-rich region is composed of a consensus repeat sequence of $(PVPPTGDSGAP)_n$, and the number of repeats marks the major difference between CEases across the species (*2*); bovine pancreatic CEase contains three such repeats, while human CEase contains 16 repeats. Studies of the proline-rich repeats show they have no role in enzymatic activity, and a physiological role for this region remains elusive (*10*−*13*). The proline-rich repeats are also serine- and threonine-rich and contain putative sites for O-glycosylation. There are also two sites for N-linked glycosylation at residues 187 and 361 (*9*, *14*).

The purpose of this study was to determine the high-resolution crystal structure of bovine pancreatic CEase to gain insight into the molecular recognition of sterols, the mechanisms of cholesterol absorption, sites of interaction

[†] This work was supported by NIH Grant GM24485 (R.M.S.).

[‡] Coordinates have been deposited in the Brookhaven Protein Data Bank under accession number 2bce and will be available within a year of publication of this paper.

[§] Graduate Group in Biophysics, University of California.

[||] Department of Biochemistry and Biophysics, University of California.

[⊥] CV Therapeutics, Inc.

[#] Present address: Department of Epidemiology, Box 357236, University of Washington, Seattle, WA 98195-7236.

[@] Present address: Dade Behring, MicroScan, 2040 Enterprise Boulevard, West Sacramento, CA 95691.

[+] Present address: Department of Medicine, Cardiology Division, Jewish Hospital of St. Louis, Washington University Medical Center, St. Louis, MO 63310.

[○] Present address: ZymoGenetics, Inc., 1201 Eastlake Avenue East, Seattle, WA 98102.

[1] Abbreviations: CEase, cholesterol esterase; CEase-C, cholesterol esterase with amino acids 574−579 deleted; PC, phosphatidylcholine; TC, taurocholate; p-NPB, *p*-nitrophenyl butyrate; HEK, human embryonic kidney; HDL, high-density lipoprotein; SDS−PAGE, sodium dodecyl sulfate−polyacrylamide gel electrophoresis; IEF, isoelectric focusing; DLS, dynamic light scattering; MES, 2-(*N*-morpholino)-ethanesulfonic acid; HEPES, *N*-(2-hydroxyethyl)piperazine-*N*′-2-ethanesulfonic acid; CHES, 2-(*N*-cyclohexylamino)ethanesulfonic acid.

S0006-2960(97)02989-9 CCC: $15.00
Published on Web 03/24/1998

with bile salt, and the mechanism of activation of this distinct lipase. Since high-resolution diffraction quality crystals could not be initially obtained from native wild-type protein (C. A. Spilburg and L. G. Lange, unpublished), the two N-linked sugars were removed by mutating asparagines 187 and 361 in the N-linked glycosylation consensus sequences to glutamines, followed by overexpression in HEK 293 cells. The purified double-mutant CEase was evaluated for electrophoretic purity (SDS−PAGE, native PAGE, and IEF), functional activity by cholesteryl oleate hydrolysis and *p*-nitrophenyl butyrate (p-NPB) hydrolysis, and oligomeric state and homogeneity by dynamic light scattering (DLS).

As this paper was being submitted, the 2.8 Å structure of the native enzyme alone and in complex with bile salt was solved independently, in a different space group (*15*). Interestingly, their apoenzyme structure is in a different conformation than our apoenzyme structure at 1.6 Å resolution, which suggests a role for the aliphatic chain of the fatty acid, mimicked by detergent in their structure, and a critical role for the C terminus in the activation of the lipase revealed in ours (*16*). Our structure shows a clear biological role for the C-terminal region of the enzyme and implicates novel structural features in the activation of this lipase.

MATERIALS AND METHODS

Cloning, Mutagenesis, and Expression. Bovine pancreatic CEase was cloned as previously described (*9*). The full-length, double-mutant CEase was constructed by first creating two single mutants, N187Q and N361Q, using PCR-based mutagenesis (*17*). N187Q was created using the mutagenic oligonucleotide 5′-GGAGACCCCGACCAAATCACCCTC-TTTG-3′, while N361Q used the oligonucleotide 5′-CTCA-GAGGTGCCGACGCCACGTACGAG-3′. The two cloned inserts were sequenced, and then cleaved with restriction enzyme *Cla*I, located between the codons for amino acids 187 and 361. The 5′ portion of N187Q and the 3′ portion of N361Q were then ligated together into a pCEP4 expression vector (Invitrogen) and expressed in HEK 293 cells as described previously (*18*).

Purification of Native and Mutant CEases. Native CEase from bovine pancreas and double-mutant N187Q/N361Q CEase expressed in HEK 293 cells were purified as previously described (*18*), with the double-mutant CEase requiring modifications. For the double mutant, 2.1 L of cell media was adjusted to 20 mM MES (pH 6.0) with 1.0 M MES, 0.45 μm filtered, and CEase precipitated by addition of ammonium sulfate (856 g to 2.1 L) with stirring for 3 h. The pellet was resuspended in 100 mL of 20 mM MES (pH 6.0) and dialyzed against 20 mM MES (pH 6.0). Following S-Sepharose chromatography [3 cm × 40 cm; equilibrated and loaded with 20 mM MES (pH 6.0), washed with 0.15 M NaCl, and CEase eluted at 0.2−0.35 M NaCl using a 0.15 to 0.6 M NaCl gradient], *p*-nitrophenyl butyrate (p-NPB, Sigma) active fractions were pooled, concentrated to approximately 10 mL, and dialyzed for 24 h against 100 mM MES (pH 6.0). The sample was applied to a 1.2 cm × 10 cm Poros CM weak cation exchanger (Perseptive Biosystems) run at 3 mL/min in 100 mM MES (pH 6.0) with 2 mL injection loads. CEase was retarded on the column with elution post flow through at 1.5−4.5 min. At 5 min postinjection, a 3.5 min gradient from 0 to 0.7 M NaCl was run to remove impurities followed by a 5 min re-equilibration. Pooled CEase was concentrated to approximately 5 mL and dialyzed against the appropriate buffer. The protein was concentrated by high-pressure stirred cell ultrafiltration using YM-10 membranes (Amicon). The protein concentration was determined by the Bradford method using bovine serum albumin as a standard.

Electrophoretic and Molecular Size Characterization. SDS−PAGE and native PAGE were performed using a Novex Xcell II Mini Cell and 4−20% acrylamide/Tris-glycine precast gels in the presence and absence of 0.1% SDS in the running buffer. Samples were prepared by mixing with an equal volume of 2× reducing application buffer (SDS−PAGE) or running buffer (native PAGE). Isoelectric focusing (IEF) was performed using precast pH 3−10 ampholite gels. IEF samples were diluted with equal volumes of IEF sample buffer. Gels were run according to Novex Precast Gel Instructions. Molecular weights and oligomeric states were assayed using the DynoPro-801 Dynamic Light Scattering Instrument equipped with a microcuvette-based MicroSampler (Protein Solutions). Prior to data collection, 1.2 mg/mL protein in 10 mM MES (pH 6.0) was filtered through a 0.02 μm Anodisc membrane using the MicroFilter system (Protein Solutions). Software version 3.00 was used for instrument control and data collection.

Enzymatic Activity Assays. Functional activities of both native and mutant CEases were assayed by monitoring the hydrolysis of cholesteryl oleate and p-NPB as a function of pH, enzyme concentration, and taurocholate (TC, Sigma) concentration. [1-^{14}C]Oleic acid release after a 5 min incubation period at 37 °C from vesicles containing cholesteryl [1-^{14}C]oleate (Amersham) and egg yolk phosphatidylcholine (PC, Sigma) was measured as previously described (*19*). Samples (25 ng of CEase/275 μL) were prepared by mixing 175 μL of 100 mM buffer [sodium acetate (pH 4.0 and 5.0), MES (pH 6.0), HEPES (pH 7.0), Tris (pH 8.0), and CHES (pH 9.0)], 75 μL of cholesteryl [1-^{14}C]oleate vesicles in 2.0 mM Tris (pH 7.2), ≤5.5 μL of 500 mM TC, 20 μL of CEase diluted 1000-fold in the appropriate pH buffer, and water to give a total volume of 275 μL. The rate of p-NPB hydrolysis at 25 °C was determined from the linear portion of the absorbance curve (10−70 s) at 405 nm using a Shimadzu UV-160 spectrophotometer equipped with a liquid temperature control system. CEase in 10 mM MES (pH 6.0) was diluted 50-fold in buffer (same as above) containing the appropriate TC concentration to give 0.02 mg/mL CEase. p-NPB was prepared by mixing 250 μL of fresh stock (9 μL in 1 mL of dioxane) into 25 mL of 25 mM MES (pH 6.0). The reaction was initiated by addition of 2 μL of p-NPB to 1 mL of protein solution directly in a quartz cuvette.

Crystallization and Data Collection. For crystallization, purified N187Q/N361Q CEase was dialyzed against 2 mM sodium phosphate (pH 7.0) and further concentrated to 5−6 mg/mL. Crystals were grown at room temperature in hanging drops by mixing equal volumes of protein with well buffer containing 0.1 M sodium acetate (pH 4.5), 1.5 M ammonium sulfate, and 6% 2-propanol. Crystals appeared in 5−8 days as twinned clusters of thin rods, averaging 200 μm × 60 μm × 30 μm in size, with a small number of single, untwinned crystals suitable for data collection. Data were

Table 1: Crystallographic Data

Data Collection Statistics	
space group	*C*2
unit cell dimensions	$a = 100.42$ Å, $b = 54.25$ Å, $c = 106.34$ Å, and $\beta = 104.12°$
resolution limit (Å)	1.6
observations (all)	66 076
completeness (%) (last shell)	89.1 (68.1)
redundancy	2.3
R_{sym} (%)	8.7
$\langle I/\sigma I \rangle$	11.5
Refinement and Model Statistics	
resolution (Å)	40.0−1.6
σ cutoff	2.0
reflections	41 187
R_{cryst} (%)	21.1
R_{free} (%)	25.0
amino acids	532 (1−112, 120−533, and 574−579)
non-hydrogen atoms	4324
water molecules	199
average *B*-factor (Å^2)	14.044
rms Δ bond lengths (Å)	0.007
rms Δ bond angles (deg)	1.377
Ramachandran geometry	89.4% most favored regions 10.2% allowed regions 0.2% generously allowed regions 0.2% disallowed regions

collected on a 30 cm image plate (MAR Research). Cryoprotectant of mother liquor containing 30% glycerol was applied to the crystal shortly before flash freezing in a 90 K nitrogen gas stream. A complete data set was collected on a single frozen crystal at Stanford Synchotron Radiation Laboratory beamline 7-1 ($\lambda = 1.08$ Å), with diffraction observed to the edge of the image plate at 1.6 Å resolution. Data were indexed, integrated, and scaled using DENZO and SCALEPACK with no σ cutoff, indexing in space group *C*2 with the following unit cell dimensions: $a = 100.42$ Å, $b = 54.25$ Å, $c = 106.34$ Å, and $\beta = 104.12°$, with a monomer in the asymmetric unit. A summary of data collection and refinement statistics is presented in Table 1.

Crystallography and Structure Refinement. Molecular replacement in AMoRe (*20*) was used to generate an initial map, and the model was improved by cycles of manual building in CHAIN (*21*) and refinement in XPLOR (*22*). Briefly, the primary sequences of bovine pancreatic CEase and *Torpedo californica* acetylcholinesterase were aligned and the acetylcholinesterase coordinates (PDB code 2ace) truncated to a discontinuous, 368-amino acid core corresponding to conserved regions of sequence and secondary structure (*23*). Rotation and translation searches, followed by rigid-body refinement in AMoRe, yielded an unambiguous solution and a starting R_{cryst} of 48.3%. A 7.0% set of reflections was set aside for calculation of R_{free} prior to refinement in XPLOR (*24*). An immediate bulk solvent correction followed by simulated annealing refinement reduced the R_{cryst} to 44.3%, with clear density corresponding to the primary sequence of CEase. Manual rebuilding followed by cycles of conjugate gradient minimization, simulated annealing, and temperature factor refinement (40−1.6 Å) dropped R_{cryst} and R_{free} to 21.1 and 25.0%, respectively. A bulk solvent correction was applied regularly throughout refinement. MIDAS was used for docking the cholesterol ester (*25*). Ramachandran parameters were monitored using PROCHECK (*26*).

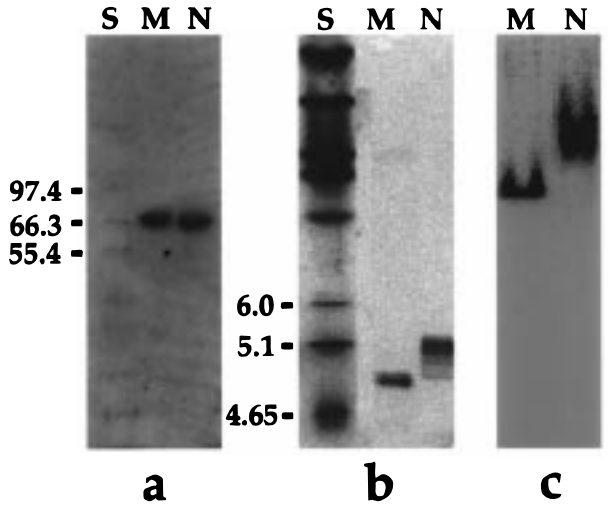

FIGURE 1: Electrophoretic characterization of mutant and native CEases: (a) SDS−PAGE, (b) IEF gel, and (c) native PAGE. Molecular weight and IEF standards are indicated by column S, and mutant and native CEases are indicated by columns M and N, respectively.

RESULTS

Protein Expression, Purification, and Characterization. The three-step purification procedure produced 5−7 mg of the purified, recombinant double mutant from 2.1 L of expression media. The purified N187Q/N361Q mutant CEase consists of one SDS−PAGE band, one native PAGE band, and three IEF bands with p*I*'s between 4.8 and 4.9 (Figure 1). In comparison, native CEase purified from bovine pancreas migrates as a single, slightly faster migrating SDS−PAGE band, a smeared, impeded multibanded pattern on native PAGE, and multiple IEF bands with p*I*'s between 4.9 and 5.1 (Figure 1). These three electrophoretic assays are indicative of glycosylation in native CEase.

Both the mutant N187Q/N361Q and native CEases exhibit essentially identical functional activity (Figure 2). Both enzymes show similar cholesteryl [1-^{14}C]oleate hydrolytic activities as a function of enzyme concentration (Figure 2a), with peak hydrolytic activity at pH 7.0 (Figure 2b). Both enzymes show similar bile salt taurocholate (TC) dependences of enzymatic activity, with half-maximal activity around 5.0 mM TC (Figure 2c). Using the water soluble ester p-NPB, both enzymes display similar profiles as a function of pH and TC concentration, with half-maximal activity at ∼0.4 mM TC at pH 7.0 (Figure 2d). Taken together, these experiments show that the presence of the N-linked sugars is not required for ester hydrolysis.

Further characterization of the purified mutant CEase by DLS yields a sample with a narrow, monomodal distribution (baseline of 0.999−1.000) of monomers, with molecular masses of 61.2 ± 1.2 and 65.5 ± 1.5 kDa, based on two independent samples of 14 and 20 measurements, respectively. This is in agreement with the calculated 63.5 kDa molecular mass of the mutant, unglycosylated enzyme. In addition, characterization of native bovine CEase also shows a homogeneous, monomodal distribution of the monomer, with an average molecular mass of 64.0 ± 3.0 kDa.

Crystal Structure. The structure was solved by molecular replacement based on a truncated model of *T. californica* acetylcholinesterase (Table 1) (*23*). CEase is a member of

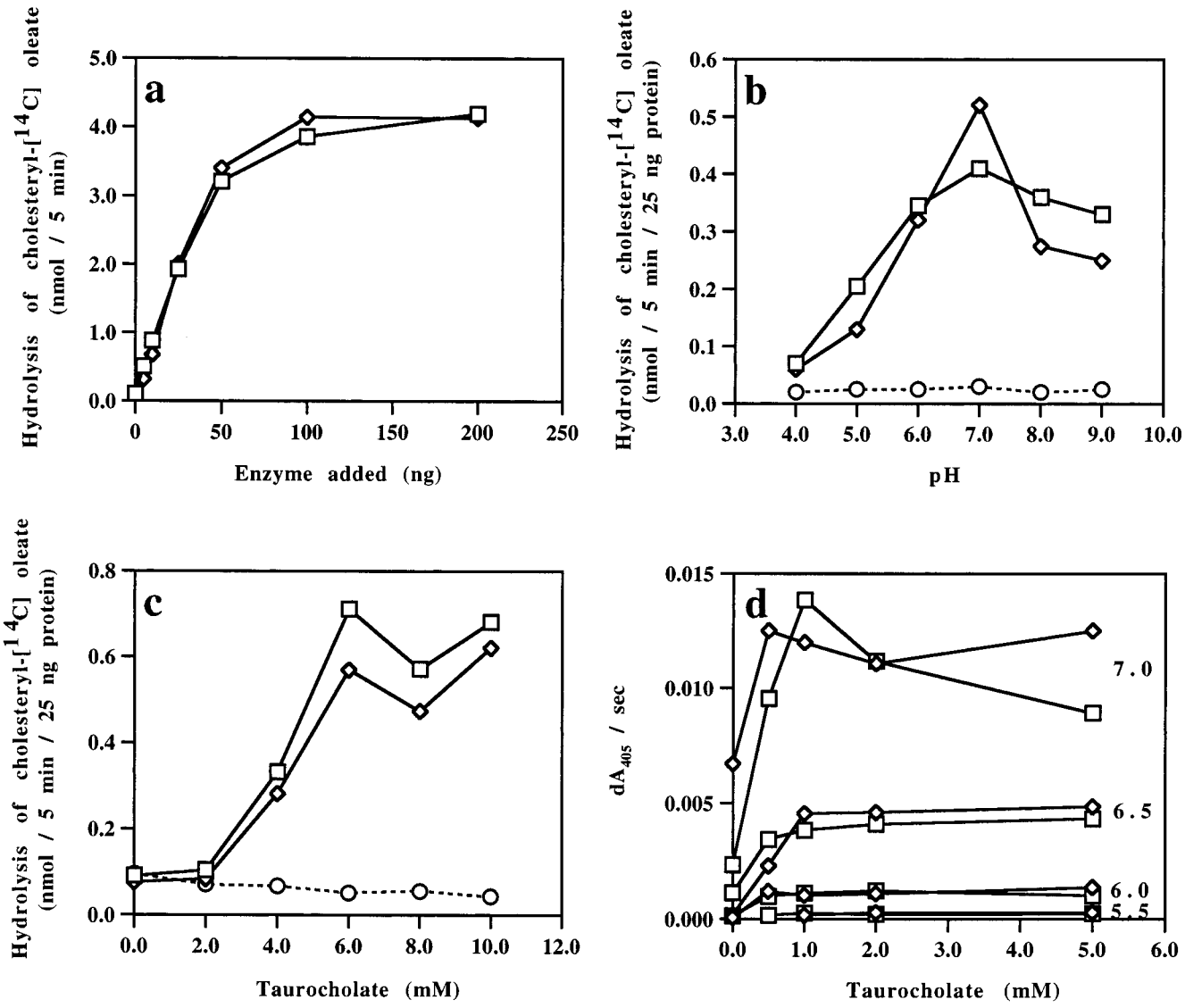

FIGURE 2: Functional analysis of mutant and native CEase. (a) Cholesteryl [1-^{14}C]oleate hydrolysis vs added enzyme. (b) Cholesteryl [1-^{14}C]oleate hydrolysis vs pH. (c) Cholesteryl [1-^{14}C]oleate hydrolysis vs TC. (d) p-NPB hydrolysis vs TC and pH. The CEase concentration was 25 ng/275 μL for cholesteryl [1-^{14}C]oleate hydrolysis experiments, in the presence of 4 mM TC. p-NPB hydrolysis experiments were performed at 0.02 mg/mL CEase. Squares and diamonds represent native and mutant CEase, respectively, and buffer blanks are indicated as circles.

the $\alpha-\beta$ hydrolase superfamily, the general fold found in esterases and other triglyceride lipase structures, typically fungal. The structure is composed of a system of 11 β-strands forming the core of the protein surrounded by 15 α-helices (Figure 3), with very clear electron density throughout the molecule (Figure 4). The catalytic triad of Asp320, His435, and Ser194 is located roughly at the center of the molecule. The unique environment around the active site residues distinguishes pancreatic CEase from other lipases (Figure 5). On the basis of homology to residues in acetylcholinesterase, Ala195, Gly107, and Ala108 of CEase are likely involved in coordinating the oxyanion intermediate in the reaction. Ala195 forms the N terminus of an 11-residue α-helix, placing it at the positive end of the helix dipole, contributing to the stabilization of the negatively charged reaction intermediate (*27*). A water molecule hydrogen bonds to the amino group of Ala195 in the apoenzyme structure. Strikingly, the extreme C terminus with its hydrophobic sequence PVVIGF is lodged in the active site (Figures 5 and 6a). The C terminus physically displaces the putative oxyanion binding residues Gly107 and Ala108 from the catalytic serine. Compared to acetylcholinesterase, the side chain of conserved Tyr105 is flipped, and the residues following veer away from the active site (Figure 6a). The hydrophobic C terminus also functions as a plug, and a calculation of accessible surface area upon removal of this hexapeptide shows that 37 mostly hydrophobic residues and 504 Å^2 of surface area are exposed. Importantly, the catalytic serine and histidine and the putative oxyanion binding residues are made more accessible to substrate (Table 2). Therefore, this C-terminal hexapeptide clearly plays a role in activation of this lipase.

CEase also lacks an amphipathic, helical lid region important for interfacial activation found in most triglyceride lipases, and instead, it is truncated into a pair of antiparallel β-strands. The N-terminal disulfide loop in CEase, containing residues 64−80, makes up this truncated lid region. A superposition of the structures of pancreatic CEase and *Candida cylindracea* CEase (*28*) clearly shows the truncation of the lid region (Figure 6b).

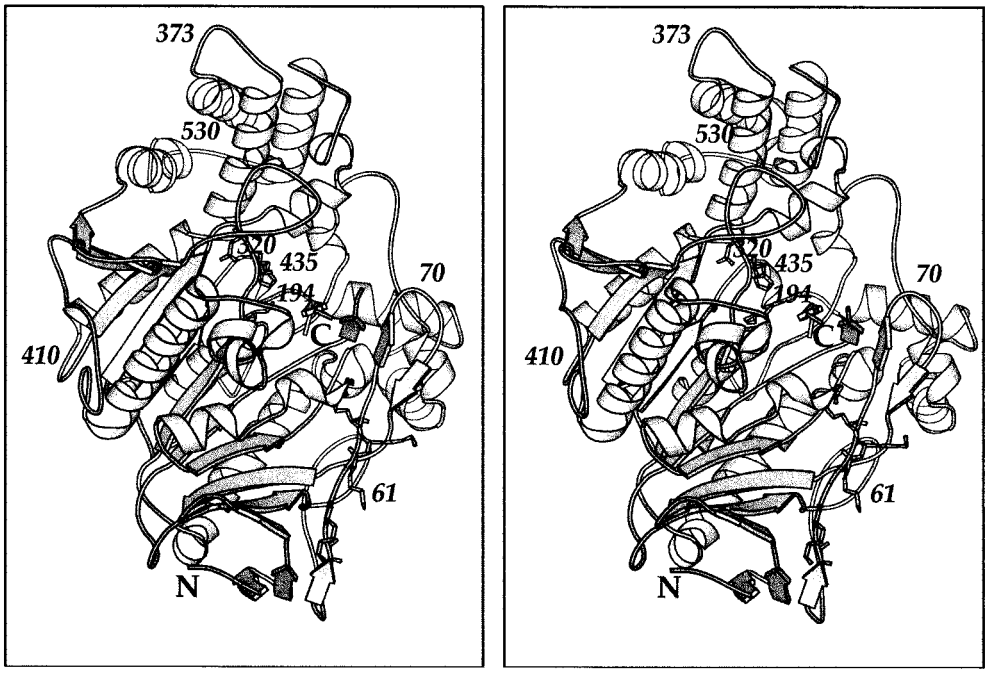

FIGURE 3: Topology and structure of bovine pancreatic CEase. The catalytic triad of Asp320, His435, and Ser194 is shown in ball-and-stick representation at the center, and the putative heparin binding domain is shown at the lower right, consisting of residues 56−63. This figure was generated using MOLSCRIPT (*40*).

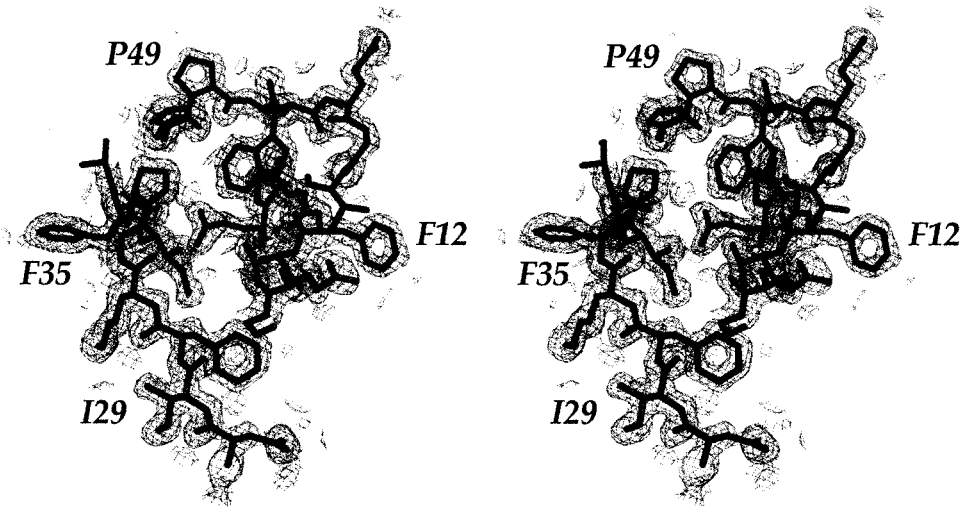

FIGURE 4: Representative N-terminal electron density. A $2F_o - F_c$ map was calculated to 1.6 Å resolution and contoured at 1σ. The map shows clear electron density in an N terminus β-sheet region of CEase. This figure was generated using MOLSCRIPT (*40*).

There are three distinct systems of β-sheets, two core systems conserved in the $\alpha-\beta$ hydrolase fold, and a unique third system lying near the active site. This third set of β-sheets is composed of four strands, amino acids 66−68 and 74−76 in the truncated lid region, amino acids 108−110, and amino acids 575−577 in the extreme C terminus (Figure 3). Immediately preceding the extreme C terminus is a proline-rich repeat region, composed of the consensus repeat sequence $(PVPPTGDSGAP)_n$, where n ranges from 3 in cows to 16 in humans (*2*). This proline-rich repeat is disordered in the electron density and presumably very flexible.

Residues 113−119 in CEase are also disordered in the electron density, corresponding to a hydrophilic loop near the active site that is conserved in all CEase sequences, but absent in other lipases and esterases. This was earlier proposed to be a bile salt binding site, and was found to be similarly disordered in the 2.8 Å apoenzyme structure (*15*).

An electrostatic potential map of the protein surface reveals unusually large patches of negative potential, with a small number of neutral and positive potential areas (Figure 7a). A conglomerate of positive charge is centered around residues 56−63, which was earlier determined to be the site of interaction with heparin-like molecules on the cell surface (*29*) (Figure 3). The primary sequence in this region, KAKSFKKR, is similar to other heparin binding sequences (*2*, *29*). This patch is located 17−30 Å from the catalytic Ser194, consistent with its proposed role of anchoring to the cell surface (*4*−*6*).

A large lobe of negative potential is proximal to the active site, in a helical domain composed of residues 322−376. In addition to this segregated distribution of charge, CEase also has an unusual distribution of temperature factors (Figure 7b). CEase shows a patch of systematically higher temperature factors also located in the helical domain

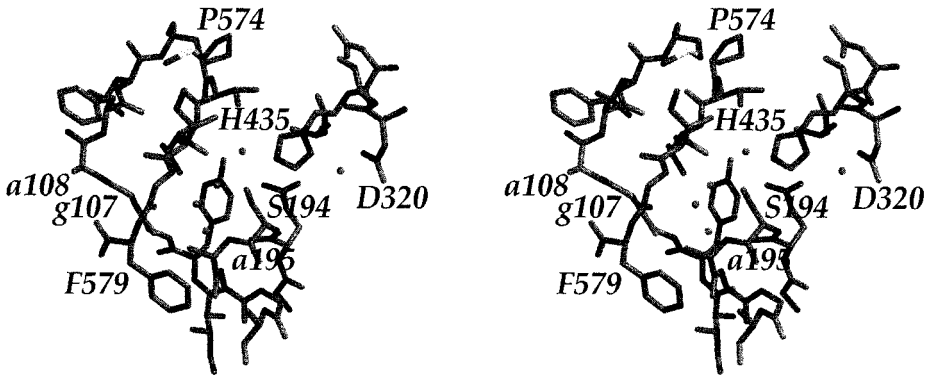

FIGURE 5: Structure of the active site region of CEase. Active site residues Ser194, Asp320, and His435 are labeled. Putative oxyanion coordinating residues Ala195, Gly107, and Ala108 are highlighted in lowercase, and C-terminal residues 574−579 are labeled. Water molecules close to Ser194 are indicated as spheres. This figure was generated using MOLSCRIPT (*40*) and Raster3D (*41*).

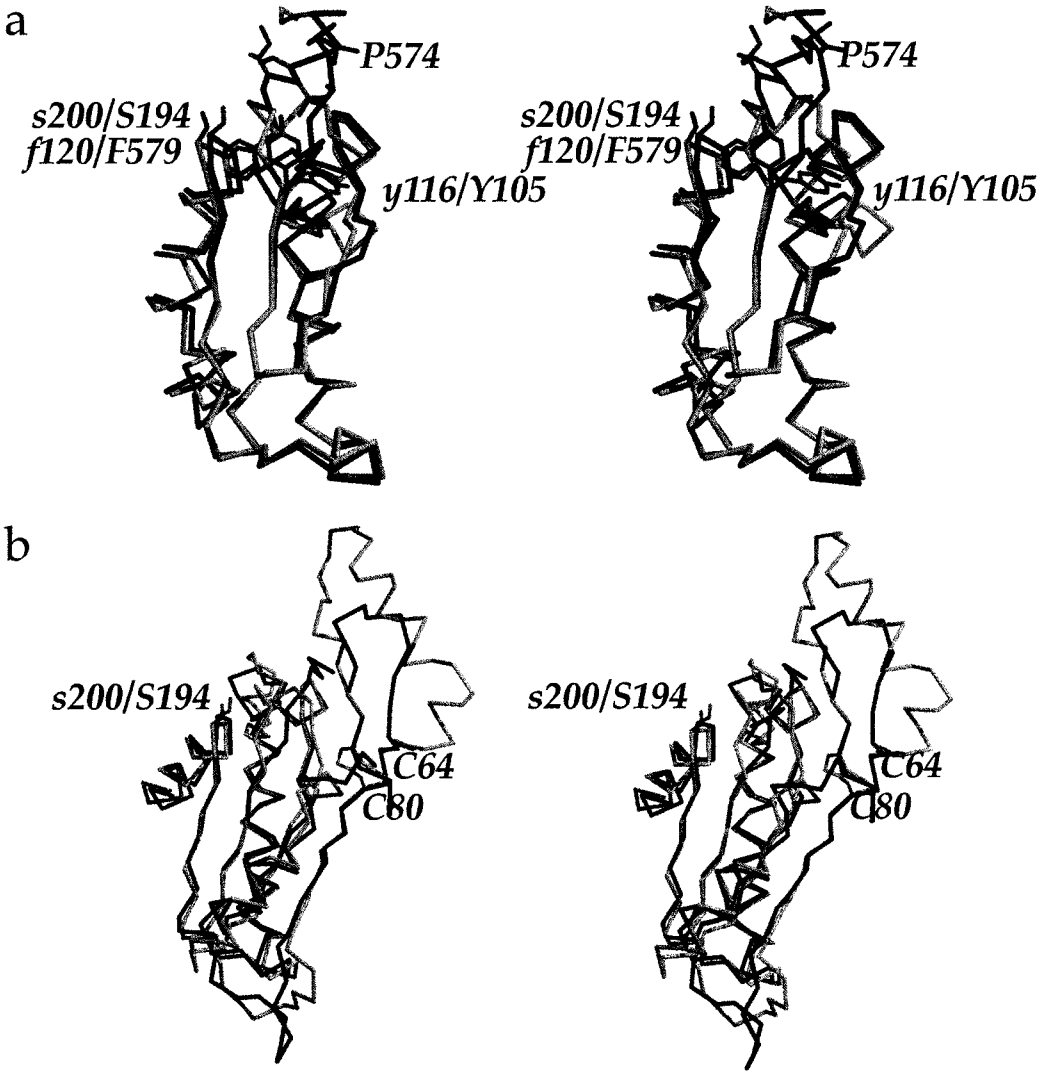

FIGURE 6: (a) α-Carbon alignment of the residues in the active site region of CEase (black) and *T. californica* acetylcholinesterase (gray). Residues in lowercase correspond to acetylcholinesterase, and residues in uppercase correspond to pancreatic CEase. Conserved Tyr105 in CEase is flipped with respect to Tyr116 in acetylcholinesterase, and the C terminus of CEase diverts the oxyanion binding loop away from catalytic Ser194 in the apoenzyme structure. The orientation of the oxyanion loop in acetylcholinesterase may represent the structure of CEase in this region in the activated state of the enzyme. (b) α-Carbon alignment of the N terminus of CEase and *C. cylindracea* CEase. Amino acids 61−210 of CEase (black) were aligned with the corresponding residues of *C. cylindracea* CEase (gray). Comparison of the regions enclosed by the N-terminal disulfide loop regions shows a truncated loop in CEase, and a helical lid in *C. cylindracea* CEase. The disulfide bridge (Cys64−Cys80) is indicated, and the active site Ser194 is shown in ball-and-stick representation. This figure was generated using MOLSCRIPT (*40*), Raster3D (*41*), and O (*42*).

containing residues 322−376. This region of higher temperature factors is strikingly coincident with the area of negative potential, suggesting a possible role for electrostatic interactions between the mixed micelle and the enzyme.

Table 2: Solvent Accessibility of Residues upon Removal of C-Terminal Residues 574−579[a]

residue	accessibility (Å^2)	accessibility after removal of peptide (Å^2)	exposed area (Å^2)
Q66	9.2	18.3	9.1
Y105	3.1	44.6	41.5
G106	8.2	15.6	7.4
G107	***0.3***	***27.3***	***27.0***
A108	***2.9***	***14.6***	***11.7***
F109	1.4	31.0	29.6
A110	14.3	30.5	16.2
M111	28.6	76.1	47.5
G112	85.4	120.6	35.2
A120	119.4	119.7	0.3
Y123	70.1	84.9	14.8
L124	9.8	30.7	20.9
Y125	8.4	10.6	2.2
Y143	5.2	7.4	2.2
V145	6.8	9.7	2.9
F150	2.0	15.3	13.3
E193	0.1	2.1	2.0
S194	**4.8**	**23.4**	**18.6**
A195	***2.0***	***38.6***	***36.6***
A198	0	4.2	4.2
S199	0	4.5	4.5
L202	1.0	1.4	0.4
W227	22.0	32.6	10.6
A228	0	1.2	1.2
Y270	6.5	10.3	3.8
L272	7.4	10.8	3.4
L282	17.2	17.3	0.1
L285	5.3	36.8	31.5
F287	8.7	15.5	6.8
V288	3.8	21.3	17.5
P289	0	12.9	12.9
L323	27.9	37.2	9.3
F324	3.9	21.2	17.3
M327	44.2	47.6	3.4
H435	**3.8**	**15.5**	**11.7**
A436	4.8	29.3	24.5
L439	5.6	7.4	1.8

[a] Catalytic residues are indicated in bold, and the putative oxyanion binding residues are in bold italics. Calculation of the solvent accessible area was carried out using ASC (*39*).

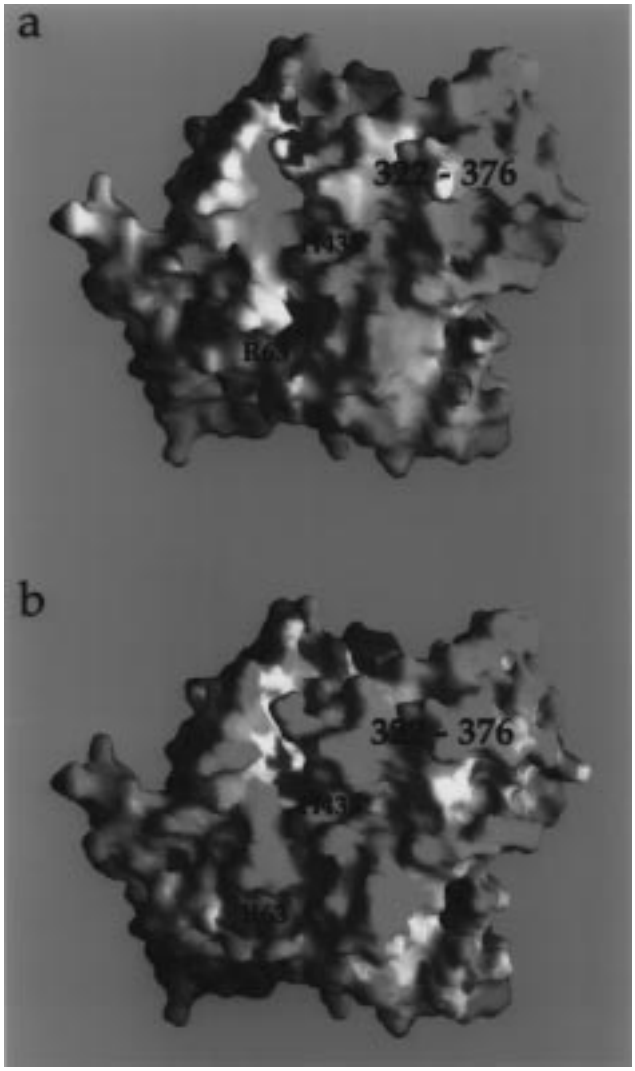

FIGURE 7: Electrostatic potential and temperature factor profiles of CEase. (a) Potential diagram ramped from $-10/kT$ (red) to $+10/kT$ (blue). The putative heparin binding site lies at the area of positive potential at the lower left, with Arg63 indicated. (b) Temperature factor diagram of the active site face of bovine pancreatic CEase. The catalytic His435 is indicated, with temperature factors ramped from blue (low temperature factors) to red (high temperature factors). The areas of high temperature factors and negative potential are coincident, notably in the helical region of amino acids 322−376 at the upper right. This figure was generated using GRASP (*43*).

DISCUSSION

Purification and Characterization of CEase. The mutation of the two N-linked glycosylation sites and the subsequent expression, purification, and functional characterization show that no N-linked oligosaccharides are involved in the hydrolytic activity of the enzyme. Electrophoretic characterization of native CEase shows that the increase in the number of isoelectric forms and average p*I* relative to those of mutant CEase, and the change in mass-to-charge ratio in native CEase, is due to the presence of the N-linked sugars. Even though the function of the N-linked sugars is not well understood, rat pancreatic CEase lacking the N-linked sugars was secreted at 50% lower levels in Chinese hamster ovary and pancreatoma cells, showing a role for glycosylation in the secretion of the enzyme in vivo (*30*, *31*). The N-linked sugars are also implicated in protein folding and the thermal stability of the enzyme (*31*). Although the amino acids in the region surrounding residues 187 and 361 are neutral to hydrophilic, the N-linked sugars may also play a role in improved solubility. We show by DLS and crystal packing that bovine CEase is a functional monomer as is human CEase (*32*). Therefore, the native CEase dimers, present in both the uncomplexed and TC-complexed structures of Wang et al., are due to crystallization conditions and crystal packing. Crucial to this study was the increased homogeneity in the double mutant. Previously, we were unable to obtain atomic resolution data from native CEase crystals, and the improvements in homogeneity brought about by the removal of the N-linked sugars may have contributed to the growth of well-ordered crystals.

A Possible Role for the C Terminus in Lipase Activation. The structure of CEase at 1.6 Å resolution shows an $\alpha-\beta$ hydrolase with an unusual active site region, where the last six amino acids of the enzyme, PVVIGF, splay the putative oxyanion hole away from the active site (Figures 5 and 6a). Defining a biological role for the C terminus has been difficult (*13*); however, the last six amino acids are highly conserved among mammalian CEases (Table 3). Therefore, we expect that the C terminus plays a similar role in the function of these enzymes. The length of the proline-rich

Table 3: Alignment of C-Terminal Residues of Mammalian CEases

bovine	EVAQMPVVIGF
human	KEAQMPAVIRF
rabbit	VAAQMPMAIGF
mouse	VEAQMPATIGF
rat	VEAQMPVAIGF

repeats preceding the C terminus varies across the mammalian CEases, with three repeats in the bovine enzyme, four in the rat enzyme, and 16 in the human enzyme. Structurally, the proline-rich repeats may act as a tether to the C terminus and may exhibit similar disorder in the structures of other mammalian CEases.

The removal of the final six amino acids (CEase-C) exposes a predominantly hydrophobic 504 Å^2 of surface area (Table 2). Manual docking of cholesteryl linoleate (PDB code 1cle) into the active site of CEase-C indicates that the alkyl chain of the fatty acid fits in the hydrophobic pocket left by the removal of the terminal amino acids, with the proper tetrahedral geometry dictated by the oxyanion intermediate (Figures 8 and 9) (*28*). Given that this probable binding mode of the cholesteryl ester occupies the same hydrophobic pocket as the C terminus, we propose that the C-terminal peptide must move to accommodate the substrate. The structure shows that this hexapeptide plays an important role in the function of this enzyme not only by displacing the oxyanion hole from the active site but also by occupying a deep hydrophobic pocket that is the proper size for accommodating the fatty acid of a cholesterol ester (Figure 8).

The truncation of the lid region in pancreatic CEase and the presence of the C-terminal peptide in the active site suggest a unique set of structural rearrangements required for lipase activation. Whether the movement of the peptide is driven by substrate, by bile salt, or by a combination of the two is unclear. The movement of the C-terminal peptide may be driven by the interaction with bile salt. As the C-terminal residues are hydrogen bonded to the mobile loop implicated in bile salt activation, binding of bile salt and the subsequent ordering of residues 113−119 may contribute to the movement of the C-terminal peptide (*33*). Furthermore, enzymatic data on native and truncated forms of CEase, where the proline-rich repeats and the hydrophobic C terminus were deleted, show lowered K_m and elevated V_{max} values for the truncated CEases relative to those of the native CEase at low, nonsaturating concentrations of bile salt (*33*). At saturating concentrations of bile salt, the truncated and native CEases are kinetically indistinguishable, and are therefore structurally indistinguishable, indicative of a displaced C terminus in the presence of bile salt (*33*). Therefore, as the enzyme binds to the bile salt, the resulting displacement of the C terminus allows the loop containing the oxyanion binding site to move into a position that can coordinate the intermediate (Figures 5 and 6a).

The movement of the C-terminal peptide may also be driven by substrate binding, as implicated by the crystal structure of the apoenzyme of CEase in the presence of detergent. Wang et al., in their structure of the apoenzyme determined independently at 2.8 Å resolution, show a preformed oxyanion hole with no density seen for the C terminus. While our construct involved mutation of two N-linked consensus glycosylation sequences, the differences in the apoenzyme structures are not due to the lack of N-linked glycosylation in our structure. The N-linked glycosylation sites are distal to the active site and C terminus, and furthermore, activity assays on the native and mutant CEases show identical enzymatic activity (Figure 2); therefore, glycosylation does not play a role in the conformational differences between our structure and that of Wang et al. In light of their structure, it appears that crystallization conditions may account for the notable differences between their apoenzyme structure and ours. The authors use the detergent zwittergent 3-12 as an additive in the crystallization. Despite the lack of interpretable detergent density in the putative fatty acid binding pocket in their structure, it is possible that the long alkyl chain of the detergent may have helped displace the C terminus from the active site, allowing the oxyanion hole to move into its productive binding position. This is consistent with the known sensitivity of the conformation of lipase structures to crystallization conditions and suggests a role for substrate in the displacement of the C terminus, as mimicked by detergent. Our crystals lack any detergent and therefore may more accurately reflect the conformation of the enzyme in the absence of bile salt and substrate. Nevertheless, the enzymatic data and the crystal structure of the apoenzyme in the presence of detergent coupled with our high-resolution apoenzyme structure point toward a clear role for the displacement of the C terminus during lipase activation.

Bile Salt Binding and Enzymatic Activity. Characterization of native and mutant CEases shows different bile salt concentration dependence curves of enzymatic activity for water soluble versus hydrophobic esters, with an observed half-maximal activation for TC of around 400 μM in the case of water soluble ester hydrolysis and half-maximal activation at a TC concentration of 5.0 mM in the case of cholesteryl oleate hydrolysis. While these numbers cannot be directly compared due to the unknown concentration of substrate in the micelle and the dynamic physical chemical properties of the mixed micelle, 5.0 mM is in the range of the critical micelle concentration of TC, suggesting a role of TC as a surfactant in addition to being an activator of CEase. From the independently determined 2.8 Å structure of the enzyme complexed with bile salt, two binding sites were found, a proximal site and a distal site. The proximal site near the catalytic triad orders residues 116−125 and swings the binding loop away from the active site, thus allowing easier access of substrate (*15*). On the basis of our apoenzyme structure, we argue that the second, distal site may be involved in opening the substrate binding pocket to accommodate the bulkier cholesterol esters. The distal bile salt binding site is located in a cleft between the helical bundle domain of residues 322−376 and the core of the enzyme. This is consistent with the temperature factor distribution of our structure, where this same helical bundle domain has systematically higher temperature factors than the remainder of the molecule (Figure 7b). This domain may be ordered by the binding of bile salt to the distal site.

An Electrostatic Role in Lipase Activation? Pancreatic CEase shows a patch of systematically higher temperature factors located in the helical domain containing residues 322−376 (Figure 7b), coincident with the area of negative

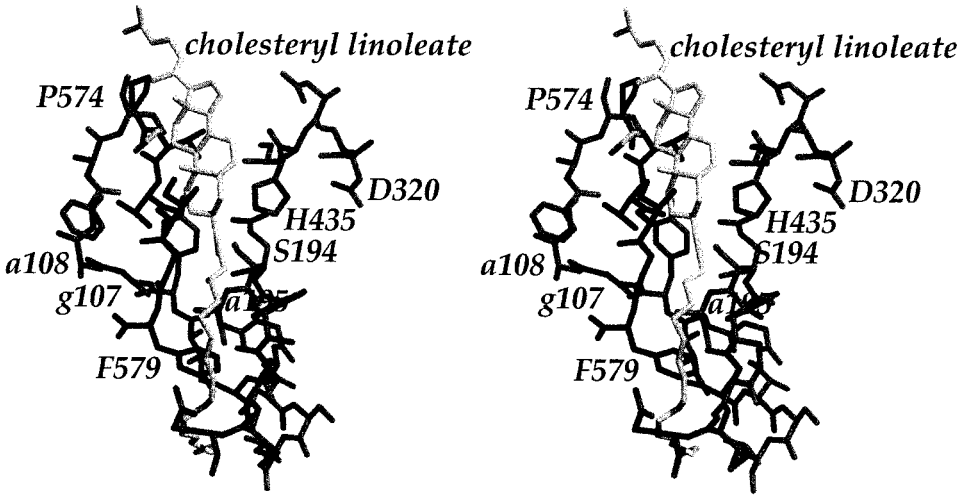

FIGURE 8: Stereodiagram of proposed Michaelis complex between CEase (black) and cholesteryl linoleate (gray). Active site residues Ser194, His435, and Asp320 are indicated, and putative oxyanion residues Ala195, Gly107, and Ala108 are in lowercase. The cholesteryl linoleate molecule spatially overlaps with C-terminal residues 574−579. Docking was done using MIDAS (*25*). This figure was generated using MOLSCRIPT (*40*) and Raster3D (*41*).

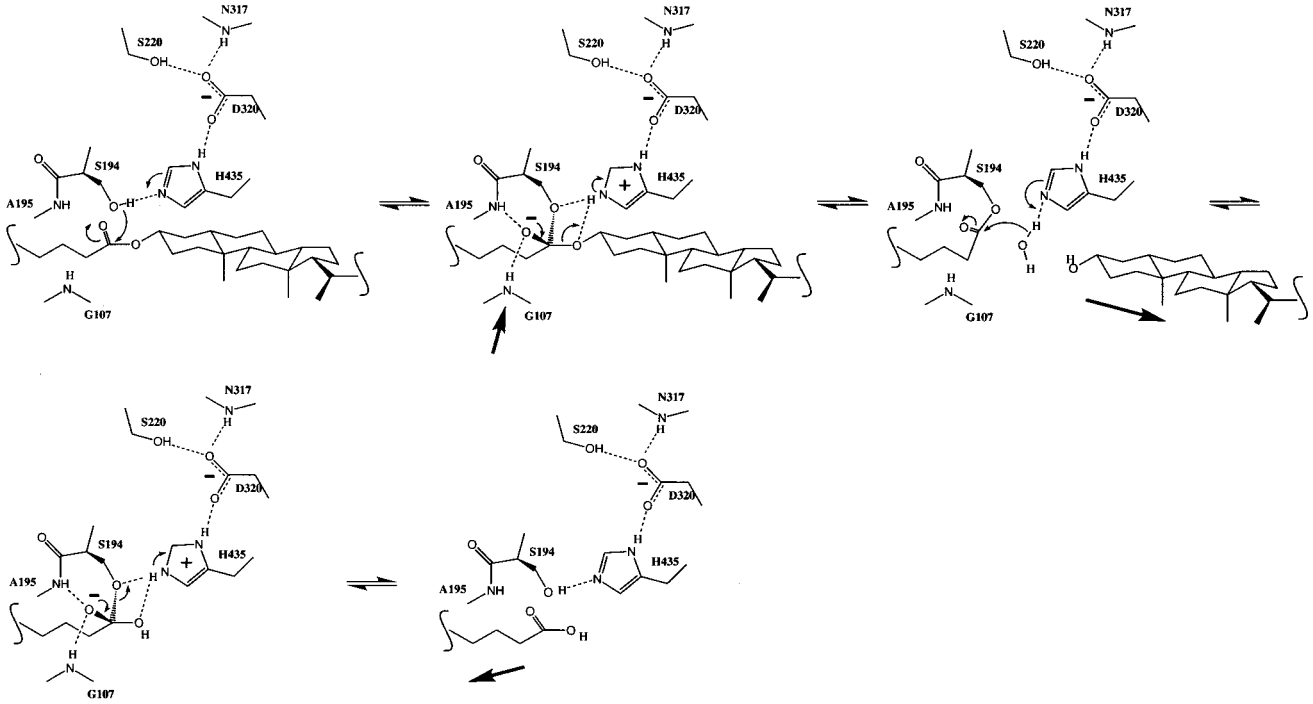

FIGURE 9: Active site hydrogen bond network and proposed mechanism and stereochemistry of the tetrahedral intermediate in the ester hydrolysis reaction. The NH of Ala195 is in a position to coordinate the oxyanion, and the loop containing Gly107 may move into a productive binding position to act as a second hydrogen bond donor to the oxyanion.

potential (Figure 7a). Because of the charged nature of the more mobile regions of the molecule, we propose a role for electrostatic interactions in binding the mixed micelle. Interactions of CEase with mixed micelles of bile salt and phospholipids, containing free cholesterol, cholesterol esters, and triglycerides, may be mediated by the positive charge on phospholipids such as phosphatidylcholine. As the phospholipids and cholesterol esters are hydrolyzed, changes to the physical chemical properties of the mixed micelle lead to dissociation from the protein. This region may thus have evolved to properly orient the enzyme face relative to the mixed micelle or guide the micelle toward the active face of the molecule.

Evolutionary Aspects. Though evolutionarily unrelated, the mechanism of hydrolysis by CEase is profoundly homologous to the mechanisms of hydrolysis of esters by the serine proteases. Therefore, the comparisons of the active site structures provide another critical assessment of the features most important to the chemical mechanisms of hydrolysis. The docking of cholesteryl linoleate into the active center allows for an assessment of contributions that may pertain to the mechanism of hydrolysis (Figure 8). From this model, the ester bond can be brought against the γO of Ser194 and the ϵN of His435 in a manner that suggests the stereochemistry of nucleophilic attack by the γO of Ser194 on the carbonyl carbon of the ester. This model predicts

that the nucleophilic attack takes place from the opposite side of the ester, leading to the inversion of chirality of the tetrahedral intermediate with respect to the trypsin-like serine proteases (Figure 9). This predicted stereochemical inversion is consistent with the structures of other triglyceride lipases in complex with inhibitors (*34*−*37*). From our docking, the hydrogen bonds from the imidazole to the γO of Ser194 and from the Nδ2 of His435 to the γO of Asp320 are essentially coplanar, making excellent hydrogen bonded geometry between them. The geometry of the catalytic triad is ideally suited for the ϵN of His435 to act first as a base for the serine proton and then as an acid to the oxygen of the cholesterol leaving group, presenting both oxygens in a coplanar manner with the plane of the imidazole. An additional similarity is the doubly hydrogen bonded support by two donors to the other oxygen of Asp320. These have direct analogues in the serine proteases; however, this oxygen lies in the opposite relative orientation with respect to the imidazole in the proteases. The oxyanion in the tetrahedral intermediate can be readily stabilized by the NH of Ala195; however, a second hydrogen bond would require the active site to close over the substrate. A primary candidate for a second bond is the NH of Gly107, once oriented in the correct direction.

CEase hydrolyzes both water soluble and hydrophobic esters, and its structure places it evolutionarily between the triglyceride lipases and the esterases. The triglyceride lipases preferentially hydrolyze hydrophobic esters and lipids, while esterases such as acetylcholinesterase function mainly on water soluble substrates. For CEase to accommodate larger, more hydrophobic esters, bile salt is required, in a dual role as a molecule binding specifically to CEase to open the active site to these bulkier molecules and as a surfactant to solubilize the hydrophobic esters, phospholipids, and triglycerides. Therefore, the bile salt dependence of CEase allows the enzyme to accommodate both hydrophilic and hydrophobic substrates.

The structure of the CEase apoenzyme suggests a new set of structural rearrangements involved in lipase activation. To date, most triglyceride lipase structures are distinguished by an amphipathic, helical lid covering the active site catalytic triad, shielding the hydrophobic binding pocket from substrate (*35*, *38*). During interfacial activation, the helical lid swings open upon contact with the hydrophobic interface, revealing a binding pocket readily accessible to substrate. There is no amphipathic lid in the structure of CEase; rather, a broader rearrangement of the tertiary structure is necessary for its physiological activity, mediated by bile salt and substrate binding. The displacement of the C terminus lodged in the active site is also necessary for substrate binding, as this reveals the hydrophobic binding site for the acid portion of the ester and allows the oxyanion hole to form properly to bind the reaction intermediate. Furthermore, the bile salt dependence of enzymatic activity coupled with these unusual structural features distinguishes CEase as a novel lipase with an unusual mode of lipase activation.

ACKNOWLEDGMENT

We thank S. L. LaPorte and Dr. Janet Finer-Moore for critical comments on the manuscript and Drs. Finer-Moore and Earl Rutenber for assistance with the structure refinement.

REFERENCES

1. Hui, D. Y. (1996) *Biochim. Biophys. Acta 1303*, 1−14.
2. Wang, C. S., and Hartsuck, J. A. (1993) *Biochim. Biophys. Acta 1166*, 1−19.
3. Mackay, K., Starr, J. R., Lawn, R. M., and Ellsworth, J. L. (1997) *J. Biol. Chem. 272*, 13380−13389.
4. Lopez-Candales, A., Bosner, M. S., Spilburg, C. A., and Lange, L. G. (1993) *Biochemistry 32*, 12085−12089.
5. Bosner, M. S., Gulick, T., Riley, D. J. S., Spilburg, C. A., and Lange, L. G. (1988) *Proc. Natl. Acad. Sci. U.S.A. 85*, 7438−7442.
6. Bosner, M. S., Gulick, T., Riley, D. J. S., Spilburg, C. A., and Lange, L. G. (1989) *J. Biol. Chem. 264*, 20261−20264.
7. Howles, P. N., Carter, C. P., and Hui, D. Y. (1996) *J. Biol. Chem. 271*, 7196−7202.
8. Li, F., Huang, Y., and Hui, D. Y. (1996) *Biochemistry 35*, 6657−6663.
9. Kyger, E. M., Wiegand, R. C., and Lange, L. G. (1989) *Biochem. Biophys. Res. Commun. 164*, 1302−1309.
10. Wang, C. S., Dashti, A., Jackson, K. W., Yeh, J. C., Cummings, R. D., and Tang, J. (1995) *Biochemistry 34*, 10639−10644.
11. Hansson, L., Blackberg, L., Edlund, M., Lundberg, L., Stromqvist, M., and Hernell, O. (1993) *J. Biol. Chem. 268*, 26692−26698.
12. Blackberg, L., Stromqvist, M., Edlund, M., Juneblad, K., Lundberg, L., Hansson, L., and Hernell, O. (1995) *Eur. J. Biochem. 228*, 817−821.
13. Downs, D., Xu, Y. Y., Tang, J., and Wang, C. S. (1994) *Biochemistry 33*, 7979−7985.
14. Sugo, T., Mas, E., Abouakil, N., Endo, T., Escribano, M.-J., Kobata, A., and Lombardo, D. (1993) *Eur. J. Biochem. 216*, 799−805.
15. Wang, X., Wang, C.-S., Tang, J., Dyda, F., and Zhang, X. C. (1997) *Structure 5*, 1209−1218.
16. Chen, J. C.-H., Miercke, L. J. W., Krucinski, J., Starr, J. R., Saenz, G., Wang, X., Spilburg, C. A., Lange, L. G., Ellsworth, J. L., and Stroud, R. M. (1997) *FASEB J. 11*, A1064.
17. Good, L., and Nazar, R. N. (1992) *Nucleic Acids Res. 20*, 4934.
18. Spilburg, C. A., Cox, D. G., Wang, X., Bernat, B. A., Bosner, M. S., and Lange, L. G. (1995) *Biochemistry 34*, 15532−15538.
19. Cox, D. G., Leung, C. K., Kyger, E. M., Spilburg, C. A., and Lange, L. G. (1990) *Biochemistry 29*, 3842−3848.
20. Navaza, J. (1994) *Acta Crystallogr. A50*, 157−163.
21. Sack, J. S. (1988) *J. Mol. Graphics 6*, 224−225.
22. Brunger, A. T. (1992) *X-PLOR: A System for X-ray Crystallography and NMR*, Yale University Press, New Haven, CT.
23. Raves, M. L., Harel, M., Pang, Y. P., Silman, I., Kozikowski, A. P., and Sussman, J. L. (1997) *Nat. Struct. Biol. 4*, 57−63.
24. Kleywegt, G. J., and Brunger, A. T. (1996) *Structure 4*, 897−904.
25. Ferrin, T. E., Huang, C. C., Jarvis, L. E., and Langridge, R. (1988) *J. Mol. Graphics 6*, 13−27.
26. Laskowski, R. A., Moss, D. S., and Thornton, J. M. (1993) *J. Mol. Biol. 231*, 1049−1067.
27. Hol, W. G. J., van Duijnen, P. T., and Berendsen, H. J. C. (1978) *Nature 273*, 443−446.
28. Ghosh, D., Wawrzak, Z., Pletnev, V. Z., Li, N., Kaiser, R., Pangborn, W., Jornvall, H., Erman, M., and Duax, W. L. (1995) *Structure 3*, 279−288.
29. Baba, T., Downs, D., Jackson, K. W., Tang, J., and Wang, C. S. (1991) *Biochemistry 30*, 500−510.
30. Morlock-Fitzpatrick, K. R., and Fisher, E. A. (1995) *Proc. Soc. Exp. Biol. Med. 208*, 186−190.
31. Abouakil, N., Mas, E., Bruneau, N., Benajiba, A., and Lombardo, D. (1993) *J. Biol. Chem. 268*, 25755−25763.
32. Loomes, K. M., and Senior, H. E. J. (1997) *FEBS Lett. 405*, 369−372.

33. DiPersio, L. P., Carter, C. P., and Hui, D. Y. (1994) *Biochemistry 33*, 3442−3448.
34. Brzozowski, A. M., Derewenda, U., Derewenda, Z. S., Dodson, G. G., Lawson, D. M., Turkenburg, J. P., Bjorkling, F., Huge-Jensen, B., Patkar, S. A., and Thim, L. (1991) *Nature 351*, 491−494.
35. Grochulski, P., Li, Y., Schrag, J. D., Bouthillier, F., Smith, P., Harrison, D., Rubin, B., and Cygler, M. (1993) *J. Biol. Chem. 268*, 12843−12847.
36. van Tilbeurgh, H., Egloff, M.-P., Martinez, C., Rugani, N., Verger, R., and Cambillau, C. (1993) *Nature 362*, 814−820.
37. Rubin, B. (1994) *Nat. Struct. Biol. 1*, 568−572.
38. Grochulski, P., Li, Y., Schrag, J. D., and Cygler, M. (1994) *Protein Sci. 3*, 82−91.
39. Eisenhaber, F., Lijnzaad, P., Argos, P., Sander, C., and Scharf, M. (1995) *J. Comput. Chem. 16*, 273−284.
40. Kraulis, P. J. (1991) *J. Appl. Crystallogr. 24*, 946−950.
41. Merritt, E. A., and Murphy, M. E. P. (1994) *Acta Crystallogr. D50*, 869−873.
42. Jones, T. A., Zou, J. Y., Cowan, S. W., and Kjeldgaard, M. (1991) *Acta Crystallogr. A47*, 110−119.
43. Nicholls, A., Sharp, K. A., and Honig, B. (1991) *Proteins 11*, 281−296.

BI972989G